Biosensors and Bioelectronics 236 (2023) 115408

Contents lists available at ScienceDirect

Biosensors and Bioelectronics

journal homepage: www.elsevier.com/locate/bios

Microneedle electrochemical aptamer-based sensing: Real-time small molecule measurements using sensor-embedded, commercially-available stainless steel microneedles

Alex M. Downs *, Adam Bolotsky, Bryan M. Weaver, Haley Bennett, Nathan Wolff, Ronen Polsky, Philip R. Miller

Biological & Chemical Sensors Department, Sandia National Laboratories, 1515 Eubank Blvd. SE, Albuquerque, New Mexico 87123, USA

ARTICLE INFO

Keywords:
Microneedle
Electrochemical aptasensors
Wearables
Microelectrodes
Continuous sensing

ABSTRACT

Microneedle sensors could enable minimally-invasive, continuous molecular monitoring – informing on disease status and treatment in real-time. Wearable sensors for pharmaceuticals, for example, would create opportunities for treatments personalized to individual pharmacokinetics. Here, we demonstrate a commercial-off-the-shelf (COTS) approach for microneedle sensing using an electrochemical aptamer-based sensor that detects the high-toxicity antibiotic, vancomycin. Wearable monitoring of vancomycin could improve patient care by allowing targeted drug dosing within its narrow clinical window of safety and efficacy. To produce sensors, we miniaturize the electrochemical aptamer-based sensors to a microelectrode format, and embed them within stainless steel microneedles (sourced from commercial insulin pen needles). The microneedle sensors achieve quantitative measurements in body-temperature undiluted blood. Further, the sensors effectively maintain electrochemical signal within porcine skin. This COTS approach requires no cleanroom fabrication or specialized equipment, and produces individually-addressable, sterilizable microneedle sensors capable of easily penetrating the skin. In the future, this approach could be adapted for multiplexed detection, enabling real-time monitoring of a range of biomarkers.

1. Introduction

Both at the hospital and at home, sensors can improve detection and management of disease. On-body monitors of blood oxygen and glucose, for example, help us to better understand and treat a range of diseases (Majumder et al., 2017; Rodbard, 2016; Vigersky, 2015). However, very few bodily processes and diseases have a suitable commercial sensor. Consequently, we still turn to lab testing for therapeutic monitoring, paneling biomarkers, and tracking disease progress. Such medical testing relies overwhelmingly on slow, invasive sampling methods, such as blood draws. In most lab-based tests, that sample then requires treatments, ranging from centrifugation and dilutions, to reagent additions and washing steps (KarenCox et al., 2019; Richard McPherson, 2021). These added steps impede direct integration of lab-based assays into wearable devices for in situ measurements. Put simply, we require more technologies that, analogous to the continuous glucose meter, can quickly measure specific biomarkers directly in the living body.

When coupled with real-time sensors, microneedle-based wearables present a promising route toward rapid, minimally painful (Miller et al., 2018; Rajabi et al., 2016) sensing directly within the body. Microneedles could enable such measurements by providing direct access to the skin's interstitial space, which holds valuable information ranging from drug distribution (Kolluru et al., 2019; Samant et al., 2020) to immune status (Tran et al., 2018). In previous reports, microneedles have been fabricated using polymers (Baek et al., 2021; Donnelly et al., 2011; Miller et al. 2011, 2014; Park et al., 2005), glass (Martanto et al., 2006; Wang et al. 2005, 2006), silicon (Dervisevic et al., 2021; Kim et al., 2018; McAllister et al., 2003; Mukerjee et al., 2004; Wilke et al., 2005; Yan et al., 2010; Yoon et al., 2013), and metals (Gill and Prausnitz, 2007; Matriano et al., 2002; Miller et al., 2018). However, stainless steel needles fashioned from commercial off the shelf (COTS) materials are a particularly promising route for producing dermal sensors. Such steel

Abbreviations: EAB sensor, electrochemical aptamer-based sensor; MN-EAB sensor, microneedle electrochemical aptamer-based sensor; KDM, kinetic differential measurement.

* Corresponding author.
E-mail address: amdowns@sandia.gov (A.M. Downs).

https://doi.org/10.1016/j.bios.2023.115408
Received 8 March 2023; Received in revised form 11 May 2023; Accepted 15 May 2023
Available online 16 May 2023

needles can penetrate the skin without excessive application force or breakage (Li et al., 2021; Rajabi et al., 2016), withstand routine sterilization, and be rapidly prototyped.

Electrochemical aptamer-based (EAB) sensors are an ideal platform for sensing in the interstitial fluid, whose protein and cellular content closely resembles whole blood (Miller et al., 2018). These sensors are among the only platform technologies that function directly in bodily fluids (Ferapontova et al., 2008; Idili et al., 2019b; Lai et al., 2007; Liu et al., 2014; Swensen et al., 2009; Xiao et al., 2005) and in situ in the living body (Arroyo-Currás et al., 2017b; Chamorro-Garcia et al., 2023; Dauphin-Ducharme et al., 2019; Idili et al. 2019a, 2021; Li et al., 2017). EAB sensors consist of an electrode-attached, redox reporter-labeled aptamer that binds to its target species (Xiao et al., 2005). When the aptamer binds to its target, a shift in electron transfer between the redox reporter and electrode occurs (Fig. 1A) (White et al., 2008). This shift, in turn, can be detected using a range of electrochemical techniques (Arroyo-Currás et al., 2018; Downs et al., 2020; Pellitero et al., 2021; Santos-Cancel et al., 2018; Xiao et al., 2005), enabling quantification with a calibration curve. Unlike many affinity assays, EAB sensors function directly in situ because they require no reagents or mixing steps. And because aptamers exist for many targets, the platform is widely generalizable to a range of biomarkers. For many aptamers, signaling reversibility allows measurements of increasing and decreasing target concentration(Dauphin-Ducharme et al., 2019; Idili et al., 2019a; Sykes and White, 2021). This reversibility makes them useful for both measurements at a single point of time, and over many hours. Indeed, recently EAB sensors have demonstrated quantification in whole blood even after 24 h (Leung et al., 2021). To date, EAB sensor development has yielded sensors that, in a wearable format, could greatly improve medical care. Specifically, real-time monitoring of high toxicity antibiotics, chemotherapeutics, and indicators of infection could improve treatment safety and efficacy for patients experiencing cancer or life-threatening infections.

Here, we create individually-addressable microneedle sensors by embedding EAB sensors within commercial-off-the-shelf (COTS) stainless steel microneedles (Fig. 2A). The device uses widely-accessible materials, and doesn't require time-consuming cleanroom fabrication or additive manufacturing. As a model system, we utilize an EAB sensor for the antibiotic, vancomycin (Dauphin-Ducharme et al., 2019). This aptamer has sufficient affinity for clinically-relevant in vivo monitoring of vancomycin (Dauphin-Ducharme et al., 2019; Downs et al., 2021), and has not demonstrated notable cross-reactivity with structurally similar compounds or interferants in the body (Dauphin-Ducharme et al., 2019). While vancomycin effectively treats serious infections, it has a narrow clinical window of safety and efficacy (6 to 42 μM) (Rybak et al., 2020; Suzuki et al., 2012). During dosing, vancomycin's toxicity often necessitates therapeutic monitoring via repeated blood draws and lab analysis (Burns and Goldman, 2020; Rybak et al., 2020). To further complicate, therapeutic drug monitoring is time-dependent and mis-timing of blood draws in clinical scenarios often impedes effective treatment (Melanson et al., 2013). Thus, microneedle-based continuous monitoring of vancomycin could improve drug administration by tracking real-time concentrations in the body and tailoring treatment to individual pharmacokinetics.

2. Materials and methods

2.1. Working electrode fabrication

We fabricate microneedle sensor electrodes using 5 cm long, 50 μm diameter, PFA-coated gold wires (A-M Systems, Sequim, WA). To form the electrode face, we trim one end of the gold wire at an approximately ~45–60° angle using a #11 surgical blade (World Precision Instruments, Sarasota, FL). Using a Keyence VHX 7000 Microscope (Keyence Corporation of America, Itasca, IL), we inspect the sensor face cut quality for smoothness and minimal PFA overhang (which can promote air bubbles following immersion). We strip the opposite side of the wire to isolate 3 mm of exposed gold for later electrical connections. We remove a 32G BD Microfine stainless steel needle (BD, Franklin Lakes, NJ) from its housing and thread the gold electrode through the blunt end of the needle. We center the exposed, angled gold face within the needle bore, and secure them by adding epoxy to the needle-wire interface at the needle's blunt end. We use urethane conformal coating (MG Chemicals, Surrey CA) for individual wire electrode testing (Figs. 3–4). To reduce breakage at the electrode-needle interface, we transition to using Double/Bubble D-85 urethane epoxy (Ellsworth Adhesives, Germantown, WI) for microneedle patch testing (Fig. 5). To form electrical connection to the sensors, we solder the wire to a gold-plated pin connector (CH Instruments, Inc., Austin, TX) with 60/40 lead-selenium solder (Digikey, Tief River Falls, MN) at the 3 mm exposed gold end. We confirm that the commercial perfluoroalkoxy (PFA) insulation on the gold wires insulates them from the microneedles by performing electrical continuity testing with a digital multimeter. We coat the solder-wire interface with either urethane conformal coating or double bubble epoxy resin to reduce breakage during handing of the delicate gold microwires.

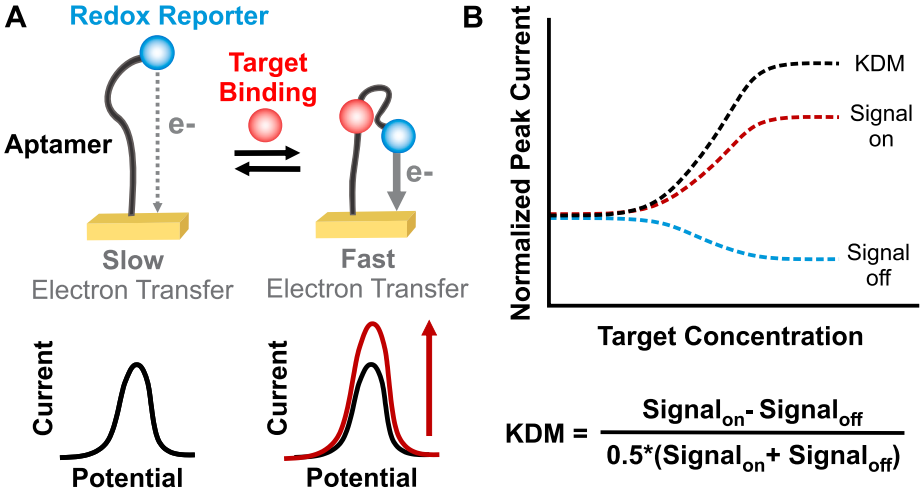

Fig. 1. (A) Most commonly, electrochemical aptamer-based (EAB) sensors consist of an aptamer (black) modified with a redox-reporter (blue) attached to a gold electrode (yellow). Upon binding of target (red), a change in electron transfer kinetics between the redox reporter and the surface occurs, which is easily monitored using square wave voltammetry as an increase (or decrease) in square wave voltammogram peak current (red). **(B)** Depending upon the square-wave frequency employed, the peak currents seen in square wave voltammetry can increase ("signal on" behavior) or decrease ("signal off") in response to target binding. To assess target binding, we titrate the sensors with known amounts of target, and measure the response at different square wave voltammetry frequencies. To increase gain and correct for the appearance of drift, we obtain Kinetic Differential Measurement (KDM) values by taking the difference in normalized peak currents collected at a signal-on and a signal-off frequency, then dividing that value by the average of the normalized signal-on and signal-off peak currents (detailed in section 2.5) (Ferguson et al., 2013).

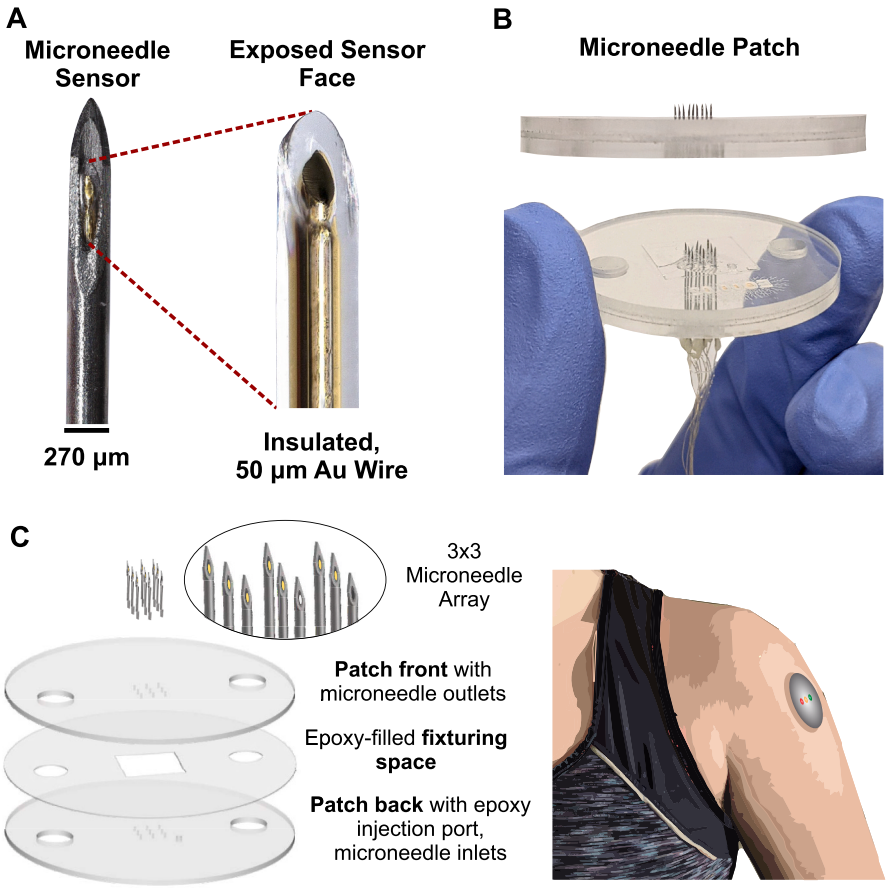

Fig. 2. (A) We utilize a commercial-off-the-shelf (COTS) approach to producing microneedle sensors. We embed a gold microwire sensor (50 µm diameter) into a 32G stainless steel insulin needle (270 µm diameter). By trimming the end of the microwire, we produce an exposed, angled gold face. On this microwire face, we conjugate an EAB sensor. **(B)** To enable wearable transdermal EAB sensing, we arrange these microneedle sensors into an array format with controlled needle length. **(C)** We secure a 3x3 array of needles (containing sensors, and a single reference and counter electrode) into a laser-cut polymethylmethacrylate (PMMA) housing. This allows penetration of the skin in a wearable format.

2.2. Microneedle reference and counter electrode fabrication

To produce an electrochemical cell compatible with wearable measurements, we miniaturize the reference and counter electrode into a microneedle format (Fig. S1). To create a counter electrode, we insert a PFA-insulated, 50 µm diameter platinum wire (A-M Systems, Sequim, WA) into a microneedle with an exposed platinum face in the same manner described in section 2.1 (Fig. 4A). The microneedle counter functions when biased against multiple sensors, which we confirm by performing vancomycin measurements in PBS for seven microneedle sensors biased against the microneedle counter electrode (Fig. S2). For a microneedle reference electrode, we achieve a stable pseudo-reference electrode using the exposed face of a 75 µm diameter, parylene-insulated silver wire modified to form AgCl (Fig. S1). To demonstrate function, we form EAB sensors within microneedles, then collect repeated square wave voltammetry measurements referenced to the AgCl. Compared to other common pseudo-reference systems, such as gold (Solchenbach et al., 2016; Thiruvottriyur Shanmugam et al., 2020) and platinum (Bond and Lay, 1986; Torriero, 2019), the AgCl produces a stable peak position (Fig. S1). Because 50 µm diameter PFA-coated silver wire was not available, we insulate silver wires in house. To do so, we cut 5 cm lengths of 75 µm diameter, PFA-coated silver wires (A-M Systems, Sequim, WA), and use a razor blade to strip the bottom 1 inch of PFA from each wire. We coat these with a 5–6 µm layer of parylene C, insert the electrode end with the thin parylene C coating into the microneedle, and assemble the electrode in the same manner as the other two substrates. To produce a layer of AgCl, we soak the microneedle/silver wire assemblies in Chlorox Disinfecting bleach for at least 1 h, then rinse them in deionized water.

2.3. Aptamer preparation

We first thaw a 2 µL aliquot of 50 µM aptamer (sequence below) modified with a 6-carbon thiol linker on the 5′ end and methylene blue on the 3’ end (Integrated DNA Technologies, Coralville, IA, dual HPLC purification, stored at −20°C).

5′-SH-$(CH_2)_6$- CGAGG GTACC GCAAT AGTAC TTATT GTTCG CCTAT TGTGG GTCGG-O-CH2- CHCH2OH-$(CH_2)_4$-NH–CO-$(CH_2)_2$-methylene blue-3′.

This aptamer (originally described in (Dauphin-Ducharme et al., 2019)) responds to the antibiotic, vancomycin, with affinity in the aptamer’s clinical range ($K_{1/2}$ = 45 µM in room temperature bovine blood (Dauphin-Ducharme et al., 2019), $K_{1/2}$ = 73 ± 4 µM in body temperature rat blood (Downs et al., 2022)).

To reduce the disulfide bonds of the aptamer constructs, we combine 7 µL of 10 mM Tris (2-carboxyethyl) phosphine (TCEP, Sigma-Aldrich, St. Louis, MO) with the aptamer sample for a 1 h thiol reduction in the dark at room temperature. We then dilute the sample with 100 µL 1X phosphate buffered saline (PBS, pH = 7.4). Here and elsewhere in our protocol, the PBS is prepared by diluting 20X PBS (Alpha Teknova, Hollister, CA) to 1X using deionized water and adding 2 mM $MgCl_2$ (Sigma-Aldrich, St. Louis, MO). We quantify the concentration of the aptamer using the molar absorption coefficient at 260 nm provided by the supplier with UV–VIS spectroscopy (DU800, Beckman Coulter, Brea, CA). Using PBS, we then dilute the aptamer to 500 nM.

2.4. Sensor preparation

For Fig. 3, our electrochemical cell contains microneedle-embedded gold sensor working electrodes, a platinum counter electrode (CH Instruments, Inc, Austin, TX), and an Ag|AgCl reference electrode (CH

Instruments, Inc., Austin TX). For Figs. 4–5, our electrochemical cell contains a microneedle-embedded gold sensor working electrode, a microneedle-embedded platinum counter electrode, and a microneedle-embedded AgCl pseudoreference electrode. We secure our working, counter, and reference electrodes in a cell vessel "shot glass" with a 3D-printed lid fixture (3D printed using Miicraft Ultra, Miicraft USA, Amityville, NY). First, we electrochemically clean the electrodes in 0.5 M NaOH (Sigma-Aldrich, St. Louis, MO) by performing repeated cyclic voltammetry scans between −1 and −1.6 V (all potentials versus Ag|AgCl) at 1 V s^{-1} scan rate for 300 cycles using a CH Multipotentiostat (CHI1040C, CH Instruments, Inc.). For these and all other electrochemical measurements, we bias all working electrodes against a single reference and counter electrode, interrogating the working electrodes simultaneously. We rinse the electrodes in deionized water, then electrochemically cycle them using cyclic voltammetry (0 to 1.8 V, 0.1 V/s) in 0.5 M H_2SO_4 (Sigma-Aldrich, St. Louis, MO). Immediately following electrochemical cleaning, we rinse the electrodes thoroughly in deionized water and place them in the prepared aptamer solution for 1 h at room temperature in dark conditions. To passivate the electrode surface, we then rinse the electrodes with deionized water and immerse them for 12 to 18 h at room temperature in 10 mM 6-mercapto-1-hexanol (Sigma-Aldrich, St. Louis, MO) suspended in 1X PBS. Following a final rinse with deionized water, the sensors are ready for use.

For Fig. 5, we perform the same electrochemical cleaning and sensor conjugation steps, but instead of using a shot glass vessel, we use a laser cut fixture to isolate a 200 μL, open face fluidic cell above the microneedle array.

2.5. Measurements and data analysis

We fill the electrochemical cell with 20 mL PBS, rinse the electrodes in deionized water, and secure them in the electrochemical cell's 3D-printed cap. Before each experiment, we collect three baseline cyclic voltammograms in PBS (−0.1 to −0.5 V versus Ag|AgCl, 0.1 V/s scan rate) to confirm redox peaks indicative of successful aptamer deposition.

To collect a calibration curve, we move the electrode cap to a vessel of the selected media held in a Lauda RE 415S temperature bath at 37°C (Lauda-Brinkmann, Delran, NJ). For bovine blood experiments, we commercially source blood from Lampire Biological Laboratories with a custom heparin formulation of 3 units/mL (Lampire Biological Laboratories, Pipersville, PA). We requested this custom formulation because we observed rapid separation of the blood at this provider's default 100 unit/mL heparin concentration. In the selected titration media, we collected square wave voltammograms (approximately −0.2 to −0.4 V versus Ag|AgCl, 25 mV amplitude) at 10 Hz and 60 Hz first in absence of target. We select these square wave frequencies because they yield signal-off and signal-on responses, respectively. After incrementally adding each target concentration, we back-pipette the electrochemical cell at least twenty times, and allow the solution to rest for approximately 2 min. In blood and other biological media, a downward drift in square wave voltammogram peak current often occurs. To correct for any peak signal loss, we apply a previously-described drift correction technique termed "Kinetic Differential Measurements" (KDM) (Ferguson et al., 2013). Here, KDM denotes when normalized signal-off peak currents are subtracted from the normalized signal-on peak currents, then divided by the average of normalized signal-on and signal-off currents (Equation 1).

$$KDM = \left(i_{norm,ON} - i_{norm,OFF}\right) / \left(0.5^{*}\left(i_{norm,ON} + i_{norm,OFF}\right)\right) \quad (1)$$

To generate a calibration curve, we collect KDM values as a function of target concentration, then fit the average normalized values to a Hill-Langmuir isotherm:

$$KDM = KDM_{min} + \left((KDM_{max} - KDM_{min})^{*}[Target]^{n_H}\right) \Big/ \left([Target]^{n_H} + \left(K_{\frac{1}{2}}\right)^{n_H}\right) \quad (2)$$

Where n_H is the Hill coefficient (a measure of binding cooperativity), $K_{1/2}$ is the midpoint of the binding curve, KDM is the KDM value observed at the applied target concentration, KDM_{min} is the KDM value seen in the absence of target, and KDM_{max} is the KDM value at saturating target concentrations. To fit the data to a Equation (2), we input titration concentrations and average, normalized KDM values into Matlab's curve fitting application. We fit the data with the constraints: (-infinity < KDM_{max} < infinity), (1e-12<$K_{1/2}$<1), (-infinity < KDM_{min} < infinity), and ($0<n_H<10$).

To perform a spiking experiment, we use a CH software macro to repeatedly collect and store square wave voltammograms as.txt files. We collect a baseline with no target, then sequentially added known amounts of vancomycin. For each addition, we back-pipette rapidly at least twenty times, while taking care not to create bubbles in the solution, then measure the resulting signal for 5 to 10 min. To analyze square wave voltammetry peak currents in real time, we use a previously reported, open-source python script (Curtis et al., 2019). When provided with voltammogram bounds (typically, −0.2 to −0.4 V) and desired Savitzky–Golay filtering (here, 10 mV), this script calculates square wave voltammogram peak height. We export data from this program to Matlab for data analysis and presentation.

We estimate the target concentrations in spiking experiments by inputting normalized KDM values and the parameters extracted from Equation (2) into:

$$[Target] = \sqrt[n_H]{\left(K_{1/2}{}^{n_H}{}^{*}(KDM - KDM_{min})\right) / (KDM_{max} - KDM)} \quad (3)$$

3. Results and discussion

3.1. Microneedle sensors respond to vancomycin in body-temperature phosphate buffered saline

When embedded within microneedles, EAB sensors ("MN-EAB sensors") respond quantitatively to their target molecule, vancomycin. Here, we use the vancomycin sensor as a model system because its application as a wearable monitor could greatly improve the standard of care for dosing this highly toxic, narrow clinical window pharmaceutical. Briefly, we form MN-EAB sensors by securing insulated 50 μm diameter gold microwires into 32G stainless steel microneedles (Fig. 2A), and depositing redox reporter-tagged aptamers and a passivating layer of 6-mercapto-1-hexanol on the exposed wire face (Fig. 1A). Collecting a titration in body temperature phosphate buffered saline (Fig. 3A), we observe MN-EAB sensor response in the pharmaceutical's clinical range (6–42 μM (Rybak et al., 2020; Suzuki et al., 2012)) (Fig. 3B). We then demonstrate continuous, quantitative measurements by dosing a set of sensors with 10, 20, and 40 μM of vancomycin, and calibrating the response to the titration curve (Fig. 3C). The sensors yield a mean calculated concentration of 9, 17 and 35 μM, with mean accuracies of 12%, 13%, and 12%, respectively (Table S1). While the sensor-to-sensor variation is greater than previous reports leveraging larger sensing electrodes (Downs et al., 2022), the measurements satisfy the required ± 20% accuracy required for vancomycin's clinical monitoring (Chavada et al., 2017; Downs et al., 2022). Thus, EAB sensors function in microneedle format, even when the working electrode is significantly miniaturized.

3.2. Microneedle sensors respond to vancomycin in undiluted, body-temperature bovine blood

Using the microneedle electrochemical cell, we demonstrate quantitative measurements in undiluted blood. Here, we use blood to validate

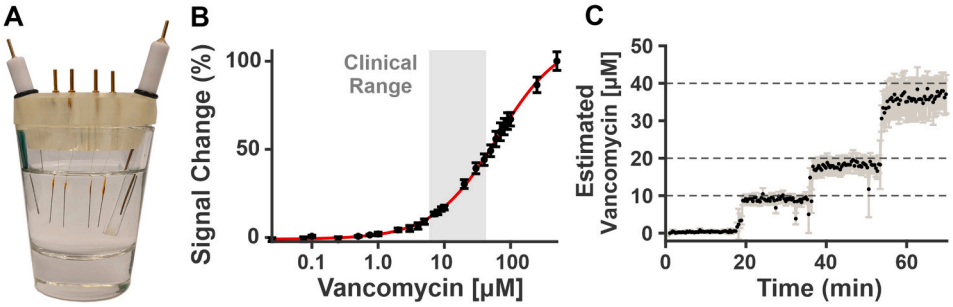

Fig. 3. Microneedle-embedded EAB sensors rapidly detect vancomycin in phosphate buffered saline (PBS). **(A)** To confirm sensor function within the microneedles, we interrogate microneedle-embedded sensors in PBS against a macro-scale Ag/AgCl reference electrode and Pt wire counter electrode. **(B)** When we expose these sensors (n = 4) to graduated amounts of vancomycin in body-temperature PBS, they produce a calibration curve with electrochemical response in the clinical range for this antibiotic target ($K_{1/2}$ = 64 ± 6 μM). **(C)** We apply this calibration curve to quantify sequential addition of 10, 20 and 40 μM vancomycin to the microneedle sensors. Here, we present the mean concentration (black) and standard error (grey) for four sensors.

the MN-EAB sensor performance due to its commercial availability, compared to interstitial fluid, and its known biofouling properties. We reason that given the similarity of the protein composition of interstitial fluid to plasma and serum (Miller et al., 2018), if the sensors function in whole blood (a more complex matrix), they will also work in interstitial fluid. Immersing the microneedle sensors, reference, and counter electrodes in body-temperature bovine blood (Fig. 4A), we produce a calibration curve for the target, vancomycin (Fig. 4B). The sensors respond in the clinical range for vancomycin (Fig. 4B). When spiked with 30 μM target, the sensors yield a mean calculated response of 29 μM and accuracy of 3% (Fig. 4C, Table S2). Thus, the microneedle sensing system can achieve quantitative measurements in body-temperature, whole blood.

3.3. MN-EAB sensor array patches penetrate porcine skin and maintain electrochemical signal during and after skin insertion

In a wearable patch format, the microneedles easily pierce the skin. To form an array amenable to wearable sensing, we bond two disks of PMMA with a 3x3 array of laser-cut holes together (Fig. 2C). We thread microneedle-electrode assemblies through the laser-cut holes, and secure them in place by passing UV-cure resin into the small square gap in the array region (Fig. 2C). To assess microneedle patch skin penetration, we gently press a microneedle patch into a section of porcine skin (a widely-accepted proxy for human skin). We then remove the patch array and stain the skin with methylene blue. Microneedles protruding ~1.3 mm from the housing reliably penetrate the skin, producing sickle shaped marks (Fig. 5A). Needles as short as ~0.52 mm also successfully penetrate the skin (Fig. S3). Images captured before and after skin insertion confirm that insertion does not visibly damage the microelectrodes or change the electrode position within the needle (Fig. S4).

The microneedle EAB sensors achieve electrochemical signal (square wave voltammetry redox peaks) within the skin. To demonstrate this, we insert a sensor array into a section of room-temperature porcine skin (microneedles protruding ~1.3 mm from array). The sensors produce electrochemical signal in the skin, as evidenced by redox peaks in the square wave voltammograms (Fig. 5B, Fig. S5). These redox peaks confirm that the sensors form electrical contact both with the skin, and between the working, reference, and counter electrodes. Under repeated, continuous square wave voltammetry scanning within the skin, the sensors produce peak signals with consistent peak positions (Fig. S6) and a stable drift-corrected baseline signal (Fig. 5C). Raw 10 and 25 Hz data collected in the skin demonstrates a peak signal loss consistent with the biofouling phase of drift (Fig. 5C) (Leung et al., 2021). This drift is easily correctable using kinetic differential

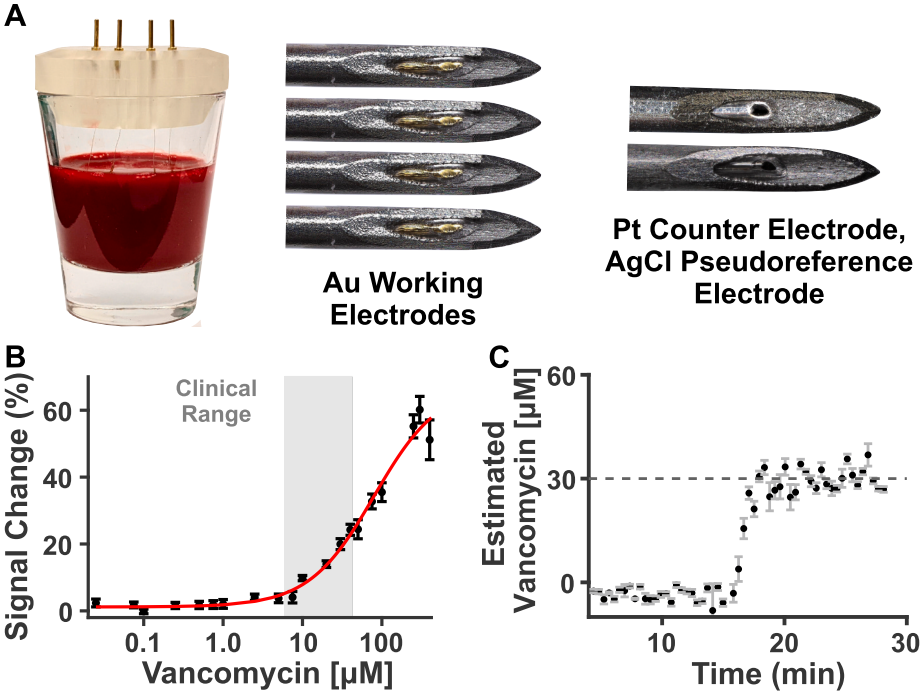

Fig. 4. We achieve real-time monitoring of vancomycin in **(A)** body temperature, undiluted whole blood, even when the electrochemical cell is miniaturized to a microneedle format (platinum microwire counter electrode, AgCl microwire pseudoreference) **(B)** When we expose the MN-EAB sensors (n = 4, interrogated simultaneously) to graduated amounts of vancomycin in whole bovine blood, they produce a calibration curve with electrochemical response in the target's clinical range ($K_{1/2}$ = 81 ± 4 μM) **(C)** We then apply this calibration curve to quantify the addition of 30 μM vancomycin to the MN-EAB sensors (n = 4, interrogated simultaneously). Here, we present the mean concentration (black) and standard error (grey) for four sensors.

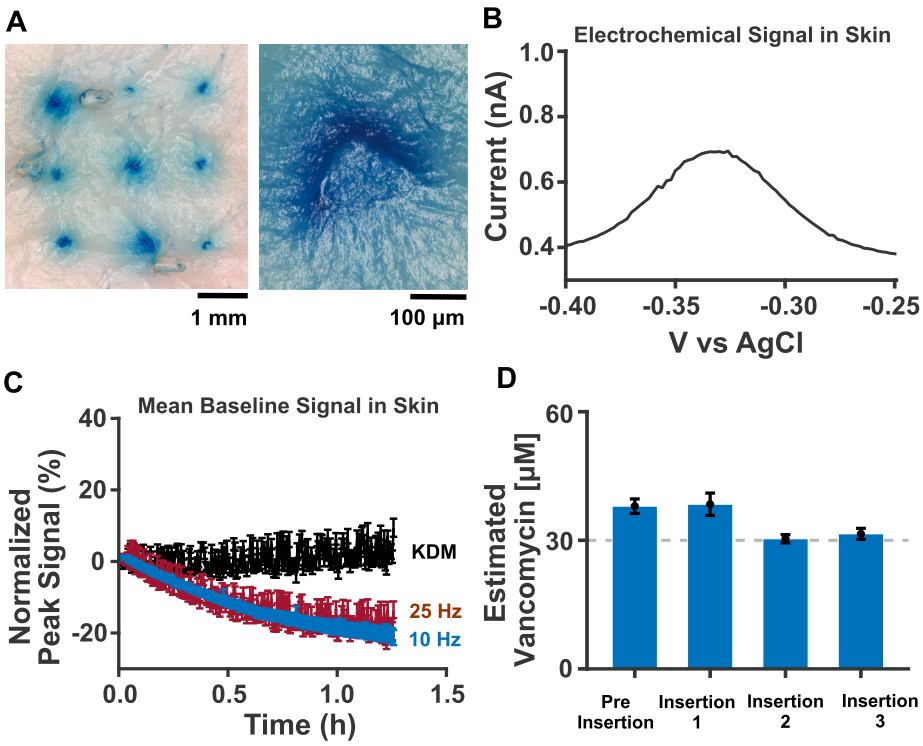

Fig. 5. The MN-EAB sensors, when implemented in a patch format, successfully penetrate porcine skin and maintain electrochemical signal during and after skin insertion. **(A)** Gently pressing a 3x3 array of ~1.3 mm long microneedles into porcine skin, we observe successful skin insertion (here, highlighted with methylene blue staining). **(B)** When we insert a MN-EAB sensor array into the skin and measure 10 Hz square wave voltammograms, we observe well-defined redox peaks (representative electrode shown here, see all five in Fig. S5). **(C)** We repeatedly interrogate an array of 5 sensors in porcine skin for >1 h. Throughout the measurement, we maintain electrochemical signal, albeit with some drift and noise. As shown by KDM measurements (black), the signal between 10 Hz (blue) and 25 Hz measurements (red) are drift correctable – providing a stable target-free baseline. **(D)** Before and after skin insertion, we dose a sensor array (n = 5 sensors) with 30 μM vancomycin in body temperature PBS. We repeat this measurement after three additional skin insertions. Here, we present the gain for the sensors before and after insertion (error bars representing standard error for five sensors).

measurements (KDM, see section 2.5), albeit with some noise present from the 25 Hz signal (Fig. S7). This noise level can be substantially reduced by smoothing the 25 Hz voltammograms using least square smoothing instead of a Savitsky-Golay filter (Fig. S8).

Skin insertion does not notably impact sensor gain or damage the sensors. To assess the impact of skin insertion on signal fidelity, we compare the sensor response to 30 μM vancomycin before and after three consecutive skin insertions (microneedles protruding ~2 mm from array). We observe electrochemical response to target both before and after insertion, even after multiple sensor insertions into the skin (Fig. 5D). The sensor accuracy varied between insertions, with respective accuracies of 27%, 28%, 1%, and 1% for the pre-insertion, and 3 post insertion target challenges (Table S3). Skin insertion itself, then, does not appear to degrade electrochemical signal or notably damage the sensors. While the first two measurements fall slightly outside of the clinical accuracy range, the latter two meet requirements for clinical monitoring. Because the sensor variation does not appear to progressively increase with insertion count, we hypothesize it does not result from insertion-induced monolayer damage. Instead, we reason that the variation observed results from sensor-to-sensor variation in the self assembled monolayer (both within the set of microneedle sensors fabricated, and between these sensors and those used in the calibration curve). This variation may appear more pronounced with the unpolished gold microelectrode surface, and may be reduced using surface area enhancement (Arroyo-Currás et al., 2017a; Downs et al., 2021).

3.4. Advantages and drawbacks of COTS microneedle sensing approach

Here, we address the advantages and drawbacks of this approach, and compare it to recently-reported microneedle electrochemical aptamer-based sensors. In the past year, there have been two reports of aptamer microneedle sensors: one that uses 3D-printed microneedles (Wu et al., 2022) and one that uses acupuncture needles electrodeposited with gold nanoparticles (Lin et al., 2022). Compared with these reports, where an entire microneedle surface is conjugated with aptamer monolayer, our sensors coat a targeted, micro-scale surface positioned within a hollow microneedle. This approach decouples the skin puncture mechanism from the EAB sensor interface. Thus, slight shifts in skin insertion depth are less likely to impact overall device function because the exposed electrode surface (which can alter electrochemical signal and impact quantification) remains constant. In contrast to 3D printed approaches, our COTS needle approach easily produces individually-addressable sensors. Each microneedle operates as its own sensor, making multiplexing straightforward. Specifically, by depositing DNA in a microwell format, we could produce microneedle patches responding to a number of different target species. To aid translation into in vivo studies commercially-available, ultra-sharp stainless steel microneedles are sterilizable, biocompatible, and can reliably penetrate the skin. Notably, needle deflection or breakage does not occur during insertion. Likewise, the needle sharpness and tailorable length allows insertion with only slight pressure.

One key drawback of our approach is a small working electrode surface area, which results in small redox currents. Because the physical area of the sensors are so small, they yield nA current, while the 3D printed and acupuncture needle approaches produce currents in the μA scale. Although this micro-scale targeted sensing surface area produces lower current, fortunately there are many routes to increase the electrodes' surface area. For example, a number of previously-described electrochemical approaches can increase the microscopic surface area anywhere from three (Arroyo-Currás et al., 2017a) to one hundred fold (Downs et al., 2021).

4. Conclusion

In this work, we present a COTS platform for microneedle measurements using electrochemical aptamer-based sensors. To validate the platform's potential for in vivo measurements, we demonstrate its function both in undiluted blood, and present a proof of concept of electrochemical signaling in porcine skin as a human skin proxy. Our microneedle sensor fabrication approach has the advantages of (1) targeted sensor measurement area, (2) individual microneedle/sensor addressability, (3) ease of needle insertion, and (4) use of widely-available, commercial materials. To enable translation into future in vivo studies, we anticipate examining the impact of sensor surface area

enhancement on measurement accuracy and noise level, and explore methods for facile multiplexing. Ultimately, this approach is an accessible method for microneedle sensing applicable both to researchers utilizing both electrochemical aptamer-based sensors and other electrochemical sensing techniques. Recognizing that EAB sensors exist for a range of targets, in the future, this COTS microneedle based approach could be adapted to measurements indicating infection or stress, and exposure to environmental hazards.

CRediT authorship contribution statement

Alex M. Downs: Conceptualization, Formal analysis, Funding acquisition, Methodology, Writing – original draft. **Adam Bolotsky:** Methodology, Writing – review and editing. **Bryan M. Weaver:** Methodology. **Haley Bennett:** Methodology. **Nathan Wolf:** Methodology. **Ronen Polsky:** Conceptualization. **Phil R. Miller:** Conceptualization, Methdology, Writing – original draft, Writing – review and editing.

Declaration of competing interest

The authors declare that they have no known competing financial interests or personal relationships that could have appeared to influence the work reported in this paper.

Data availability

Data will be made available on request.

Acknowledgements

We thank Steven Larson, Kenneth Coombes, and Patricia Sawyer for providing parylene coating services, and Kyle Klavetter for useful discussions relating to electrochemistry and electrode interfaces. We thank Sweet Mercy Farms for providing unaltered porcine skin samples. This research was supported by the Laboratory Directed Research and Development Program at Sandia National Laboratories (SAND2023-04153J). Sandia National Laboratories is a multimission laboratory managed and operated by Technology & Engineering Solutions of Sandia, LLC, a wholly owned subsidiary of Honeywell International Inc., for the U.S. Department of Energy's National Nuclear Security Administration under contract DE-NA0003525. This article has been authored by employees of National Technology & Engineering Solutions of Sandia, LLC under Contract No. DE-NA0003525 with the U.S. Department of Energy (DOE). The employees own all right, title and interest in and to the article and are solely responsible for its contents. The United States Government retains and the publisher, by accepting the article for publication, acknowledges that the United States Government retains a non-exclusive, paid-up, irrevocable, world-wide license to publish or reproduce the published form of this article or allow others to do so, for United States Government purposes. The DOE will provide public access to these results of federally sponsored research in accordance with the DOE Public Access Plan https://www.energy.gov/downloads/doe-public-access-plan. This paper describes objective technical results and analysis. Any subjective views or opinions that might be expressed in the paper do not necessarily represent the views of the U.S. Department of Energy or the United States Government.

Appendix A. Supplementary data

Supplementary data to this article can be found online at https://doi.org/10.1016/j.bios.2023.115408.

References

Arroyo-Currás, N., Scida, K., Ploense, K.L., Kippin, T.E., Plaxco, K.W., 2017a. High surface area electrodes generated via electrochemical roughening improve the signaling of electrochemical aptamer-based biosensors. Anal. Chem. 89 (22), 12185–12191.

Arroyo-Currás, N., Somerson, J., Vieira, P.A., Ploense, K.L., Kippin, T.E., Plaxco, K.W., 2017b. Real-time measurement of small molecules directly in awake, ambulatory animals. Proc. Natl. Acad. Sci. USA 114 (4), 645–650.

Arroyo-Currás, N., Dauphin-Ducharme, P., Ortega, G., Ploense, K.L., Kippin, T.E., Plaxco, K.W., 2018. Subsecond-Resolved molecular measurements in the living body using chronoamperometrically interrogated aptamer-based sensors. ACS Sens. 3 (2), 360–366.

Baek, J.Y., Kang, K.M., Kim, H.J., Kim, J.H., Lee, J.H., Shin, G., Jeon, J.G., Lee, J., Han, Y., So, B.J., Kang, T.J., 2021. Manufacturing Process of Polymeric Microneedle Sensors for Mass Production. Micromachines.

Bond, A.M., Lay, P.A., 1986. Cyclic voltammetry at microelectrodes in the absence of added electrolyte using a platinum quasi-reference electrode. J. Electroanal. Chem. Interfacial Electrochem. 199 (2), 285–295.

Burns, A.N., Goldman, J.L., 2020. A moving target—vancomycin therapeutic monitoring. J.Pediatr. Infect.Dis.Soc. 9 (4), 474–478.

Chamorro-Garcia, A., Gerson, J., Flatebo, C., Fetter, L., Downs, A.M., Emmons, N., Ennis, H.L., Milosavić, N., Yang, K., Stojanovic, M., Ricci, F., Kippin, T.E., Plaxco, K. W., 2023. Real-time, seconds-resolved measurements of plasma methotrexate in situ in the living body. ACS Sens. 8 (1), 150–157.

Chavada, R., Ghosh, N., Sandaradura, I., Maley, M., Van Hal, S.J., 2017. Establishment of an AUC0–24 threshold for nephrotoxicity is a step towards individualized vancomycin dosing for methicillin-resistant Staphylococcus aureus bacteremia. Antimicrob. Agents Chemother. 61 (5), e02535, 02516.

Curtis, S.D., Ploense, K.L., Kurnik, M., Ortega, G., Parolo, C., Kippin, T.E., Plaxco, K.W., Arroyo-Currás, N., 2019. Open source software for the real-time control, processing, and visualization of high-volume electrochemical data. Anal. Chem. 91 (19), 12321–12328.

Dauphin-Ducharme, P., Yang, K., Arroyo-Currás, N., Ploense, K.L., Zhang, Y., Gerson, J., Kurnik, M., Kippin, T.E., Stojanovic, M.N., Plaxco, K.W., 2019. Electrochemical aptamer-based sensors for improved therapeutic drug monitoring and high-precision, feedback-controlled drug delivery. ACS Sens. 4 (10), 2832–2837.

Dervisevic, M., Alba, M., Adams, T.E., Prieto-Simon, B., Voelcker, N.H., 2021. Electrochemical immunosensor for breast cancer biomarker detection using high-density silicon microneedle array. Biosens. Bioelectron. 192, 113496.

Donnelly, R.F., Majithiya, R., Singh, T.R.R., Morrow, D.I.J., Garland, M.J., Demir, Y.K., Migalska, K., Ryan, E., Gillen, D., Scott, C.J., Woolfson, A.D., 2011. Design, optimization and characterisation of polymeric microneedle arrays prepared by a novel laser-based micromoulding technique. Pharmaceut. Res. 28 (1), 41–57.

Downs, A.M., Gerson, J., Ploense, K.L., Plaxco, K.W., Dauphin-Ducharme, P., 2020. Subsecond-Resolved molecular measurements using electrochemical phase interrogation of aptamer-based sensors. Anal. Chem. 92 (20), 14063–14068.

Downs, A.M., Gerson, J., Hossain, M.N., Ploense, K., Pham, M., Kraatz, H.-B., Kippin, T., Plaxco, K.W., 2021. Nanoporous gold for the miniaturization of in vivo electrochemical aptamer-based sensors. ACS Sens. 6 (6), 2299–2306.

Downs, A.M., Gerson, J., Leung, K.K., Honeywell, K.M., Kippin, T., Plaxco, K.W., 2022. Improved calibration of electrochemical aptamer-based sensors. Sci. Rep. 12 (1), 5535.

Ferapontova, E.E., Olsen, E.M., Gothelf, K.V., 2008. An RNA aptamer-based electrochemical biosensor for detection of theophylline in serum. J. Am. Chem. Soc. 130 (13), 4256–4258.

Ferguson, B.S., Hoggarth, D.A., Maliniak, D., Ploense, K., White, R.J., Woodward, N., Hsieh, K., Bonham, A.J., Eisenstein, M., Kippin, T.E., Plaxco, K.W., Soh, H.T., 2013. Real-time, aptamer-based tracking of circulating therapeutic agents in living animals. Sci. Transl. Med. 5 (213), 213ra165-213ra165.

Gill, H.S., Prausnitz, M.R., 2007. Coated microneedles for transdermal delivery. J. Contr. Release 117 (2), 227–237.

Idili, A., Arroyo-Currás, N., Ploense, K.L., Csordas, A.T., Kuwahara, M., Kippin, T.E., Plaxco, K.W., 2019a. Seconds-resolved pharmacokinetic measurements of the chemotherapeutic irinotecan in situ in the living body. Chem. Sci. 10 (35), 8164–8170.

Idili, A., Parolo, C., Ortega, G., Plaxco, K.W., 2019b. Calibration-free measurement of phenylalanine levels in the blood using an electrochemical aptamer-based sensor suitable for point-of-care applications. ACS Sens. 4 (12), 3227–3233.

Idili, A., Gerson, J., Kippin, T., Plaxco, K.W., 2021. Seconds-Resolved, in situ measurements of plasma phenylalanine disposition kinetics in living rats. Anal. Chem. 93 (8), 4023–4032.

Karen, L., Cox, B., Viswanath Devanarayan, PhD., Kriauciunas, Aidas, Joseph Manetta, B. S., Chahrzad Montrose, PhD., Sittampalam, Sitta, 2019. Assay Guidance Manual. Eli Lilly & Company and the National Center for Advancing Translational Sciences.

Kim, H., Theogarajan, L.S., Pennathur, S., 2018. A repeatable and scalable fabrication method for sharp, hollow silicon microneedles. J. Micromech. Microeng. 28, 035007.

Kolluru, C., Williams, M., Yeh, J.S., Noel, R.K., Knaack, J., Prausnitz, M.R., 2019. Monitoring drug pharmacokinetics and immunologic biomarkers indermal interstitial fluid using a microneedle patch. Biomed. Microdevices 21 (1), 14.

Lai, R.Y., Plaxco, K.W., Heeger, A.J., 2007. Aptamer-based electrochemical detection of picomolar platelet-derived growth factor directly in blood serum. Anal. Chem. 79 (1), 229–233.

Leung, K.K., Downs, A.M., Ortega, G., Kurnik, M., Plaxco, K.W., 2021. Elucidating the mechanisms underlying the signal drift of electrochemical aptamer-based sensors in whole blood. ACS Sens. 6 (9), 3340–3347.

Li, H., Dauphin-Ducharme, P., Arroyo-Currás, N., Tran, C.H., Vieira, P.A., Li, S., Shin, C., Somerson, J., Kippin, T.E., Plaxco, K.W., 2017. A biomimetic phosphatidylcholine-

terminated monolayer greatly improves the in vivo performance of electrochemical aptamer-based sensors. Angew. Chem. Int. Ed. 56 (26), 7492–7495.
Li, H., Wu, G., Weng, Z., Sun, H., Nistala, R., Zhang, Y., 2021. Microneedle-based potentiometric sensing system for continuous monitoring of multiple electrolytes in skin interstitial fluids. ACS Sens. 6 (6), 2181–2190.
Lin, S., Cheng, X., Zhu, J., Wang, B., Jelinek, D., Zhao, Y., Wu, T.-Y., Horrillo, A., Tan, J., Yeung, J., Yan, W., Forman, S., Coller, H.A., Milla, C., Emaminejad, S., 2022. Wearable microneedle-based electrochemical aptamer biosensing for precision dosing of drugs with narrow therapeutic windows. Sci. Adv. 8 (38), eabq4539.
Liu, J., Wagan, S., Dávila Morris, M., Taylor, J., White, R.J., 2014. Achieving reproducible performance of electrochemical, folding aptamer-based sensors on microelectrodes: challenges and prospects. Anal. Chem. 86 (22), 11417–11424.
Majumder, S., Mondal, T., Deen, M.J., 2017. Wearable sensors for remote health monitoring. Sensors 17 (130), 1–45.
Martanto, W., Moore, J.S., Kashlan, O., Kamath, R., Wang, P.M., O'Neal, J.M., Prausnitz, M.R., 2006. Microinfusion using hollow microneedles. Pharmaceut. Res. 23 (1), 104–113.
Matriano, J.A., Cormier, M., Johnson, J., Young, W.A., Buttery, M., Nyam, K., Daddona, P.E., 2002. Macroflux® microprojection array patch technology: a new and efficient approach for intracutaneous immunization. Pharmaceut. Res. 19 (1), 63–70.
McAllister, D.V., Wang, P.M., Davis, S.P., Park, J.-H., Canatella, P.J., Allen, M.G., Prausnitz, M.R., 2003. Microfabricated needles for transdermal delivery of macromolecules and nanoparticles: fabrication methods and transport studies. Proc. Natl. Acad. Sci. USA 100 (24), 13755–13760.
Melanson, S.E.F., Mijailovic, A.S., Wright, A.P.M., Szumita, P.M., Bates, D.W., Tanasijevic, M.J., 2013. An intervention to improve the timing of vancomycin levels. Am. J. Clin. Pathol. 140 (6), 801–806.
Miller, P.R., Gittard, S.D., Edwards, T.L., Lopez, D.M., Xiao, X., Wheeler, D.R., Monteiro-Riviere, N.A., Brozik, S.M., Polsky, R., Narayan, R.J., 2011. Integrated carbon fiber electrodes within hollow polymer microneedles for transdermal electrochemical sensing. Biomicrofluidics 5 (1), 013415.
Miller, P.R., Xiao, X., Brener, I., Burckel, D.B., Narayan, R., Polsky, R., 2014. Microneedle-based transdermal sensor for on-chip potentiometric determination of K +. Adv. Healthc. Mater. 3 (6), 876–881.
Miller, P.R., Taylor, R.M., Tran, B.Q., Boyd, G., Glaros, T., Chavez, V.H., Krishnakumar, R., Sinha, A., Poorey, K., Williams, K.P., Branda, S.S., Baca, J.T., Polsky, R., 2018. Extraction and biomolecular analysis of dermal interstitial fluid collected with hollow microneedles. Commun.Biol. 1 (1), 173.
Mukerjee, E.V., Collins, S.D., Isseroff, R.R., Smith, R.L., 2004. Microneedle array for transdermal biological fluid extraction and in situ analysis. Sensor Actuator Phys. 114 (2), 267–275.
Park, J.-H., Allen, M.G., Prausnitz, M.R., 2005. Biodegradable polymer microneedles: fabrication, mechanics and transdermal drug delivery. J. Contr. Release 104 (1), 51–66.
Pellitero, M.A., Curtis, S.D., Arroyo-Currás, N., 2021. Interrogation of electrochemical aptamer-based sensors via peak-to-peak separation in cyclic voltammetry improves the temporal stability and batch-to-batch variability in biological fluids. ACS Sens. 6 (3), 1199–1207.
Rajabi, M., Roxhed, N., Shafagh, R.Z., Haraldson, T., Fischer, A.C., Wijngaart, W.v.d., Stemme, G., Niklaus, F., 2016. Flexible and stretchable microneedle patches with integrated rigid stainless steel microneedles for transdermal biointerfacing. PLoS One 11 (12), e0166330.
Richard McPherson, M.P., 2021. Henry's Clinical Diagnosis and Management by Laboratory Methods, 24 ed. Elsevier.
Rodbard, D., 2016. Continuous glucose monitoring: a review of successes, challenges, and opportunities. Diabetes Technol. Therapeut. 18 (S2). S2-3-S2-13.
Rybak, M.J., Le, J., Lodise, T.P., Levine, D.P., Bradley, J.S., Liu, C., Mueller, B.A., Pai, M. P., Wong-Beringer, A., Rotschafer, J.C., Rodvold, K.A., Maples, H.D., Lomaestro, B., 2020. Therapeutic monitoring of vancomycin for serious methicillin-resistant Staphylococcus aureus infections: a revised consensus guideline and review by the American society of health-system pharmacists, the infectious diseases society of America, the pediatric infectious diseases society, and the society of infectious diseases pharmacists. Clin. Infect. Dis. 71 (6), 1361–1364.
Samant, P.P., Niedzwiecki, M.M., Raviele, N., Tran, V., Mena-Lapaix, J., Walker, D.I., Felner, E.I., Jones, D.P., Miller, G.W., Prausnitz, M.R., 2020. Sampling interstitial fluid from human skin using a microneedle patch. Sci. Transl. Med. 12 (571), eaaw0285.
Santos-Cancel, M., Lazenby, R.A., White, R.J., 2018. Rapid two-millisecond interrogation of electrochemical, aptamer-based sensor response using intermittent pulse amperometry. ACS Sens. 3 (6), 1203–1209.
Solchenbach, S., Pritzl, D., Kong, E.J.Y., Landesfeind, J., Gasteiger, H.A., 2016. A gold micro-reference electrode for impedance and potential measurements in lithium ion batteries. J. Electrochem. Soc. 163 (10), A2265.
Suzuki, Y., Kawasaki, K., Sato, Y., Tokimatsu, I., Itoh, H., Hiramatsu, K., Takeyama, M., Kadota, J., 2012. Is peak concentration needed in therapeutic drug monitoring of vancomycin? A pharmacokinetic-pharmacodynamic analysis in patients with methicillin-resistant ***Staphylococcus aureus*** pneumonia. Chemotherapy 58 (4), 308–312.
Swensen, J.S., Xiao, Y., Ferguson, B.S., Lubin, A.A., Lai, R.Y., Heeger, A.J., Plaxco, K.W., Soh, H.T., 2009. Continuous, real-time monitoring of cocaine in undiluted blood serum via a microfluidic, electrochemical aptamer-based sensor. J. Am. Chem. Soc. 131 (12), 4262–4266.
Sykes, K.S., White, R.J., 2021. Measuring practical reversibility of surface-bound DNA for mechanistic insight into folding-based sensors. J. Electrochem. Soc. 168 (11), 116511.
Thiruvottriyur Shanmugam, S., Trashin, S., De Wael, K., 2020. Gold-sputtered microelectrodes with built-in gold reference and counter electrodes for electrochemical DNA detection. Analyst 145 (23), 7646–7653.
Torriero, A.A., 2019. Understanding the differences between a quasi-reference electrode and a reference electrode. Med. Anal. Chem. Int. J. 3 (3).
Tran, B.Q., Miller, P.R., Taylor, R.M., Boyd, G., Mach, P.M., Rosenzweig, C.N., Baca, J.T., Polsky, R., Glaros, T., 2018. Proteomic characterization of dermal interstitial fluid extracted using a novel microneedle-assisted technique. J. Proteome Res. 17 (1), 479–485.
Vigersky, R.A., 2015. The benefits, limitations, and cost-effectiveness of advanced technologies in the management of patients with diabetes mellitus. J. Diabetes Sci. Technol. 9 (2), 320–330.
Wang, P.M., Cornwell, M., Prausnitz, M.R., 2005. Minimally invasive extraction of dermal interstitial fluid for glucose monitoring using microneedles. Diabetes Technol. Therapeut. 7 (1), 131–141.
Wang, P.M., Cornwell, M., Hill, J., Prausnitz, M.R., 2006. Precise microinjection into skin using hollow microneedles. J. Invest. Dermatol. 126 (5), 1080–1087.
White, R.J., Phares, N., Lubin, A.A., Xiao, Y., Plaxco, K.W., 2008. Optimization of electrochemical aptamer-based sensors via optimization of probe packing density and surface chemistry. Langmuir 24 (18), 10513–10518.
Wilke, N., Mulcahy, A., Ye, S.R., Morrissey, A., 2005. Process optimization and characterization of silicon microneedles fabricated by wet etch technology. Microelectron. J. 36 (7), 650–656.
Wu, Y., Tehrani, F., Teymourian, H., Mack, J., Shaver, A., Reynoso, M., Kavner, J., Huang, N., Furmidge, A., Duvvuri, A., Nie, Y., Laffel, L.M., Doyle III, F.J., Patti, M.-E., Dassau, E., Wang, J., Arroyo-Currás, N., 2022. Microneedle aptamer-based sensors for continuous, real-time therapeutic drug monitoring. Anal. Chem. 94 (23), 8335–8345.
Xiao, Y., Lubin, A.A., Heeger, A.J., Plaxco, K.W., 2005. Label-free electronic detection of thrombin in blood serum by using an aptamer-based sensor. Angew Chem. Int. Ed. Engl. 44 (34), 5456–5459.
Yan, G., Warner, K.S., Zhang, J., Sharma, S., Gale, B.K., 2010. Evaluation needle length and density of microneedle arrays in the pretreatment of skin for transdermal drug delivery. Int. J. Pharm. 391 (1), 7–12.
Yoon, Y., Lee, G.S., Yoo, K., Lee, J.-B., 2013. Fabrication of a microneedle/CNT hierarchical micro/nano surface electrochemical sensor and its in-vitro glucose sensing characterization. Sensors 16672–16681.